INT. J. REMOTE SENSING, 1997, VOL. 18, NO. 4, 955–970

Estimating surface radiation fluxes in the Arctic from TOVS brightness temperatures

A. J. SCHWEIGER

Applied Physics Laboratory, Polar Science Center, University of Washington, Seattle, Washington 98195, U.S.A.

J. R. KEY

Department of Geography, Boston University, 147 Bay State Road, Boston, Massachusetts 02215, U.S.A.

(*Received 25 January 1996; in final form 20 June 1996*)

Abstract. A new method for estimating downwelling shortwave and longwave radiation fluxes in the Arctic from TOVS brightness temperatures has been developed. The method employs a neural network to bypass computationally intensive inverse and forward radiative transfer calculations. Results from two drifting ice camps (CEAREX, LeadEx) and from one coastal station show that downwelling fluxes can be estimated with r.m.s. errors of 20 Wm^{-2} for longwave radiation and 35 Wm^{-2} for shortwave radiation. Mean errors are less than 4 Wm^{-2} and are well within the bounds required for many climate process studies.

1. Introduction

The lack of sufficient quantitative knowledge of the Arctic surface radiation budget has been identified as an obstacle to a better understanding of the Arctic atmosphere–ice–ocean system within the global climate (World Maritime Organization/World Climate Research Programme 1992). The U.S. interagency Surface Heat Budget of the Arctic Ocean (SHEBA) (Moritz *et al.* 1993) initiative identifies as one of its primary objectives the documentation of the Arctic surface radiation budget. In particular, ice–ocean modelling studies typically use components of the surface radiation budget derived from parameterizations and climatologies. Data assimilation schemes designed to obtain statistics on the ice thickness distribution, an important climate indicator, require an ice growth rate that depends on the surface radiation balance. Climatological values of questionable quality are currently used to specify the surface radiation budget. In most cases these values do not vary in space, and vary in time only at a very coarse resolution. Even though long-term surface observations of radiative fluxes from Russian drifting stations exist, their spatial coverage is very limited. In order to construct two-dimensional fields of surface radiative fluxes, satellite data must be utilized.

In this paper we describe a method to estimate downwelling longwave and shortwave fluxes in the Arctic. The method employs an artificial neural network (ANN) to compute the relationship between radiative fluxes measured at the surface and brightness temperatures from the High Resolution Infrared Radiation Sounder (HIRS) and the Microwave Sounding Unit (MSU) components of the TIROS Operational Vertical Sounder (TOVS). Results and comparisons with surface observations from two field experiments, LeadEx and CEAREX, and one arctic coastal station, Barrow, Alaska, are presented.

2. Background

One approach to obtaining radiative fluxes at the surface from satellites is to compute them from the vertical temperature and humidity profiles, cloud conditions, and surface properties using a radiative transfer model. Due to the presence of errors in the measurements and frequently encountered non-unique solutions, the retrieval of these variables from satellite has to be treated as an estimation problem (Rodgers 1976). Values for these geophysical parameters are obtained from satellite radiances via algorithms and models that divide the estimation of surface fluxes from satellite into a multistage estimation problem. The algorithms are usually variations on the following components: (*a*) scene identification (clear/cloudy); (*b*) retrieval of surface radiative properties (temperature and reflectance), (*c*) retrieval of column optical properties (atmospheric profile, cloud optical thickness, cloud height); and (*d*) computation of downwelling surface radiation or flux profiles. This approach is often termed 'physical', even though it is better described as 'physical–statistical', since statistical constraints have to be used to allow a solution to the profile retrieval problem (Rogders 1976) and scene identification frequently includes the use of empirically determined thresholds (Kergomard *et al.* 1993, Schweiger and Key 1994, Rossow and Zhang 1995). For brevity and consistence with the literature we refer to methods that include physics in the estimation as 'physical'.

An alternative approach is to relate observed top-of-the-atmosphere (TOA) radiances directly to simultaneous ground measurements of downwelling radiation. This is usually achieved through multiple regression techniques, and is therefore empirical or statistical (Morcrette and Deschamps 1986, Schmetz 1989). The physical approach appears more attractive because once the underlying physical principles are identified, it offers the opportunity for further development of the individual components and allows for direct comparison with variables calculated in an atmospheric model, e.g., a general circulation model (GCM). Further, the inclusion of physics may be used to find a solution to the estimation problem, which minimizes the estimation error and is therefore optimal for the problem. (A statistical approach can only provide an optimal solution for the given data set.) A physical approach naturally requires that data for all the relevant variables are available and known within defined accuracy limits. But this is the problem: in the Arctic, most of the relevant variables, such as cloud fraction, cloud microphysical properties, surface albedo and temperature, are poorly validated or have been measured only for limited areas and short periods of time. Moreover, the inversion of high resolution temperature and humidity profiles from a sounding system with broad weighting function such as the HIRS-2 is fundamentally an ill-conditioned problem. Maximum likelihood estimates used to compute solutions to the inversion problem are sensitive to the selection of a first guess profile. Similarly, the retrieval of cloud optical properties involves the resolution of non-unique solutions of the inversion problem, especially for thin cloud over the highly reflective surfaces typical of the polar regions (Key and Stone 1995).

We have previously used a physical approach to calculate surface radiative fluxes in the Arctic from the International Satellite Cloud Climatology Project (ISCCP) data set (Schweiger and Key 1994). Through sensitivity studies we found that few of the input variables are known well enough to achieve a desirable accuracy of $5\,W\,m^{-2}$ on a monthly time scale. More recent work has shown substantial progress in the area of physical retrieval algorithms using TOVS and AVHRR sensor systems (Francis 1994, 1995, Key and Stone 1995). However, more research and thorough validation are required before reliable algorithms will be available that retrieve surface radiative fluxes at all times and everywhere in the Arctic and that do not

require substantial tuning, which can introduce significant biases. In addition, physical retrieval methods commonly impose a significant computational burden, since both inverse and forward radiative transfer calculations need to be performed. Performing these calculations for a multiyear data set using radiative transfer models with the required degree of sophistication—even for a limited area such as the polar regions—presents a formidable computational task. This paper therefore explores an empirical approach incorporating physically relevant satellite and surface observations that promises to deliver accurate surface radiation fluxes in the Arctic, yet is computationally efficient enough to force ice–ocean models.

3. Methodology

3.1. *What is a neural net?*

Artificial neural networks (ANNs) were initially used by neuroscientists in an attempt to understand certain functions of the brain. Over the past decade they have increasingly been applied to tasks involving the recognition of complex patterns such as signal processing, optical character recognition, and even stock market forecasting. Neural networks have also been used in a variety of remote sensing applications. ANNs have been applied to classification of Arctic clouds from the AHVRR sensor (Key *et al.* 1989, Lee *et al.* 1990, Tovinkere *et al.* 1993), and for the retrieval of temperature profiles from the TOVS and SSM/T sounding systems (Escobar *et al.* 1993, Butler and Meredith 1992). Although a variety of ANN architectures has been created, the three-layer back-propagation network is the most popular and is the architecture used in this research. Such networks consist of interconnected units (nodes) that are organized in three layers: an input, an output, and a hidden layer. Information in a neural network is processed by passing activation along connections between individual nodes. This is done by calculating the activation A of node i as the weighted sum of the activations at the connected nodes N:

$$A_i = f\left(\sum_N w_n A_n\right) \tag{1}$$

where w_{in} is the weight for the connection between nodes i and n, and f is the a nonlinear function called the activation function. Frequently a sigmoid function is used

$$f(A) = \frac{1}{1+\exp(-A)} \tag{2}$$

As the network is presented with an input pattern, activation at the input nodes is propagated over the hidden nodes resulting in a pattern at the output nodes. Initially the weights between individual nodes are random and no information is contained in the network. Adjusting the weights w_{in} for connections between nodes is called the 'learning' process. An ANN can be viewed as a vector function $\mathbf{O} = \mathbf{F}(\mathbf{I})$, where $\mathbf{O}$ is the vector of output unit activities and $\mathbf{I}$ is the input unit vector. In a back-propagation network, 'learning' is achieved simply by finding the weights w_{in} so as to minimize the difference between a presented training pattern and $\mathbf{O}$. This learning cycle involves the repetitive simultaneous presentation of matching input and output patterns while the weights are adjusted using a gradient descent search. Thus a neural network can also be viewed as a non-linear numerical optimization procedure. Characteristics of neural networks that make them attractive for the research presented here are: (1) they can, theoretically, determine any computable function; (2) they handle noisy data well; (3) no assumptions about the statistical

distribution of input variables are made; and (4) they are extremely fast. However, since neural network-based estimation methods do not include any assumptions about the underlying non-linear physics, estimates can only be truly optimal with respect to the training data set and estimation errors need to be determined through the application to an independent test or validation data set.

3.2. *Network configuration*

The neural network used in this research is a standard three-layer feed-forward network with a single layer of four hidden units. A logistic activation function and the backpropagation with momentum learning functions (Rummelhart *et al.* 1986) are used. The input layer consists of 27 nodes. Input nodes correspond to brightness temperatures from the 19 HIRS longwave (3·7 μm–15·0 μm) channels, four MSU microwave channels (53·73–57·95 GHz), the scaled visible band reflectance provided by HIRS channel 20 (0·68 μm), the cosines of the sensor scan angle and the solar zenith angle. An additional input node holds the satellite identification number and is needed to account for differences in the sensor systems between satellites. The characteristics of the TOVS sensor are given in Kidwell (1995). The output nodes correspond to the spectrally integrated longwave and shortwave fluxes at the surface. The present network has only a single four-node hidden layer. The choice of the optimal network configuration, specifically the number of hidden layer and units is an area of ongoing research and debate. It is related to the complexity of the problem, acceptable errors, training time, and the number of available training cases. A network with a larger number of hidden units has a larger number of adjustable parameters (weights of connections and biases of units) and is usually capable of finding a better solution (smaller error) for the training cases, but does not generalize well and may perform poorly on an independent set of test cases. The goal is therefore to construct and train a network that produces an acceptable error in the test set and has 'generalized' the problem. Although methods have been developed for constructing networks that generalize well, the network architecture used in the present work was determined by experimentation. Because of the large number of free parameters (the network used has 116 links + 6 biases = 122) and the relatively small number of training cases (315 for CEAREX and LeadEx combined), generalization error was minimized using stopped training (Finnoff *et al.* 1993).

3.3. *Why do we expect this to work?*

In order for a neural network to 'generalize' over a particular problem rather than just 'memorize' each individual case, it has to be presented with the appropriate information to perform this task. Clearly, if there is no relationship between TOVS brightness temperatures and downwelling radiative fluxes at the surface, the network will not be able to learn this task. Although one may approach this problem by providing an input feature vector that contains many types of possibly related information, it is clearly desirable to first examine the physical principles upon which the network is to operate. The TOVS was designed primarily for the retrieval of temperature and humidity profiles, and several algorithms have been established to invert TOVS sensor radiances. Recent improvements in the 3I retrieval algorithms (Claud *et al.* 1989, Francis 1994, 1995) have demonstrated that TOVS radiances can be used to derive temperature and humidity profiles over more problematic polar surfaces. Francis (1995) further demonstrated that a combination of HIRS channels can be used to obtain information on cloud-type and cloud-phase, and to estimate

cloud physical thickness and cloud droplet effective radius for certain types of clouds. Recent theory by Nakajima and King (1990), adapted and applied to polar surfaces by Key and Stone (1995), has shown the capability of the AVHRR sensor (TOVS contains the relevant AVHRR channels) to simultaneously retrieve cloud optical thickness and cloud effective droplet size. In addition, statistical relationships between brightness temperatures and surface radiative fluxes can be exploited by the network. For example, a statistical relationship exists between TOVS MSU channel 2 and observed ice surface temperatures under cloudy skies during winter (Francis 1994) and can be explained by the 'radiation boundary layer' theory of Overland and Guest (1991).

In order to demonstrate that a ANN can learn the individual steps in the calculation of surface radiation flux calculations a number of experiments were conducted. Escobar *et al.* (1995) have previously shown that the retrieval of temperature and humidity profiles from TOVS can be performed using a ANN. Figures 1(*a*) and 1(*b*) demonstrate the capability of a ANN to compute cloud optical properties over arctic surfaces from AVHRR radiances. The figures were generated by training an ANN on the input and output data generated using the methodology described by Key and Stone (1995). This algorithm uses one absorbing and one non-absorbing wavelength to simultaneously retrieve the cloud particle effective radius and the visible optical depth (Nakajima and King 1990). An ANN can also perform the forward radiative transfer calculations needed to calculate downwelling shortwave and longwave fluxes. Using a two-stream radiative transfer model (Key 1996) with a wide variety of atmospheric and surface conditions, training and test data sets of surface radiative fluxes were computed. An ANN was then trained using cloud particle effective radius, cloud optical depth, cloud top temperature and height, surface temperature and albedo, solar zenith angle, near-surface vapour pressure, and total aerosol optical depth as input. Results are shown in figures 2(*a*) and 2(*b*) for the downwelling surface shortwave and longwave fluxes, respectively.

It is certainly possible to use the networks discussed above in a serial fashion as a substitution for the algorithm that they were trained on. This would have the advantage that intermediate variables would still be generated and would provide a substantial gain in processing speed over their algorithmic implementations. However, an algorithm implemented in this fashion would also inherit all the shortcomings of the physical algorithms discussed above. In this paper we present results from a network that bypasses these intermediate steps.

One of the most important variables determining downwelling longwave flux (DWL) is the height of the cloud base. For a thin single-layer cloud, cloud base height can be calculated if cloud optical thickness, the cloud droplet size distribution and cloud top height are known. However, if clouds become optically thick this relation reaches a limit. Figure 3 shows modelled broadband downwelling short and longwave fluxes for a range of cloud fractions and cloud physical thicknesses. These computations were made for a low lying cloud using a two-stream model (Key 1996, Schweiger and Key 1994) by assuming constant cloud optical properties and temperature profiles. Figure 3 shows that the problem of obtaining cloud physical thickness can be constrained if cloud fraction is known (from HIRS brightness temperatures) and both shortwave and longwave downwelling radiation fluxes at the surface are available from observations. The network can therefore use this information to 'learn' a value for cloud base height for situations where the cloud optical thickness becomes too large.

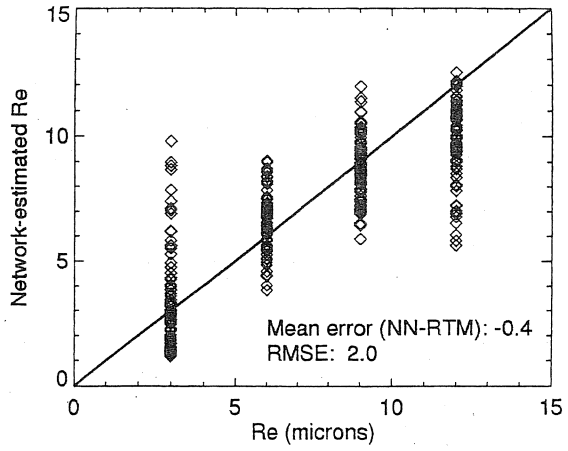

(*a*)

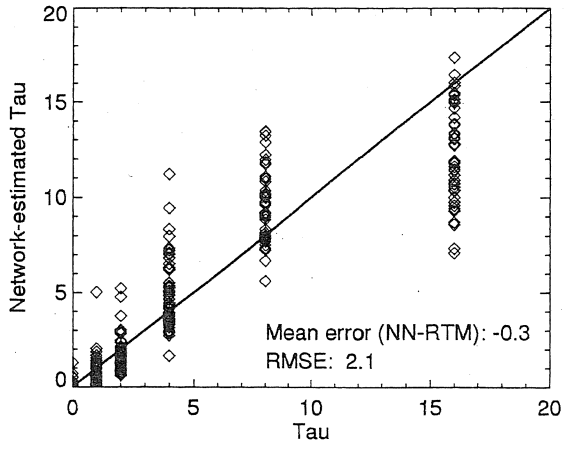

(*b*)

Figure 1. Performance of a neural network (NN) trained to invert (*a*) optical depth and (*b*) cloud droplet effective radius from AVHRR channels 2 and 3 (0·9 and 3·7 μm, respectively). Input parameters are the reflectances in these two channels, the surface albedo, aerosol optical depth, solar zenith angle, and the sensor scan angle. Input reflectance values are computed using a discrete ordinate radiative transfer model (RTM).

4. Data

Results are presented for three separate time periods and locations: the Co-ordinated Eastern ARctic Experiment from 19 September 1988 through 12 December 1988 (CEAREX Drift Group 1990) (figure 4) and the LeadEx experiment in the Beaufort Sea (figure 5) from 24 March 1992 through 4 April 1992 (LeadEx Group 1993). The CEAREX time period took place for the most part during the polar night, so only a few measurements of downwelling shortwave fluxes from the beginning of the period are available. Measurements were made at a drifting ice camp and on the research vessel *Polarbjøern* using an Eppley pyrgeometer. The

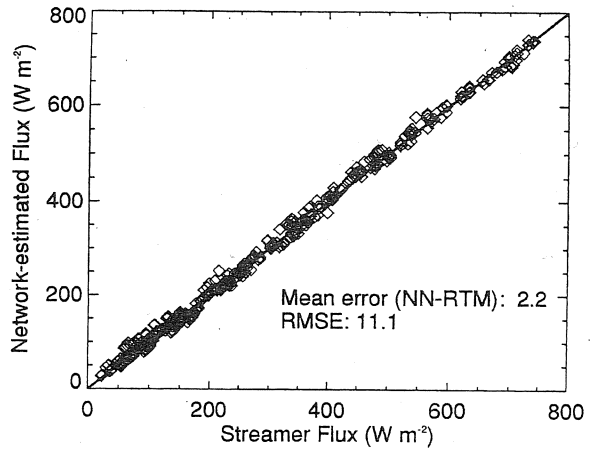

(*a*)

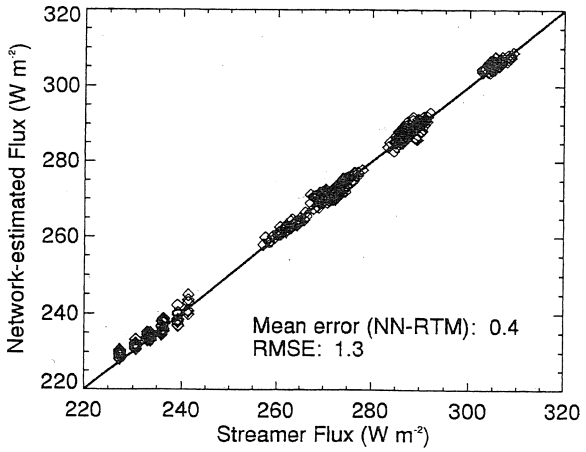

(*b*)

Figure 2. Performance of a neural net (NN) trained to estimate (*a*) downwelling shortwave and (*b*) longwave fluxes using surface temperature and albedo, cloud physical and optical properties, illumination geometry, and atmospheric aerosols and water vapour. Fluxes estimated with the neural network are compared with those computed with a two-stream radiative transfer model (RTM).

data were corrected for dome temperature, and frost and snow were removed manually. Data were averaged over 10 min intervals. Measurements during the LeadEx period were also made at a drifting ice camp. Shortwave and longwave measurements were made at 10 s intervals and averaged to 1 h intervals, also using Eppley instruments (Ruffieux *et al.* 1995). Measurements from the LeadEx and CEAREX experiments were combined to yield a data set (hereafter referred to as ICE) representing conditions over sea ice. A data set representing coastal conditions was also compiled using 1 h average meteorological and radiation observations made at Barrow, Alaska (R. Stone, personal communication, 1995). A 5 month subset (January 1992 through May 1992) is used for training a neural network performing

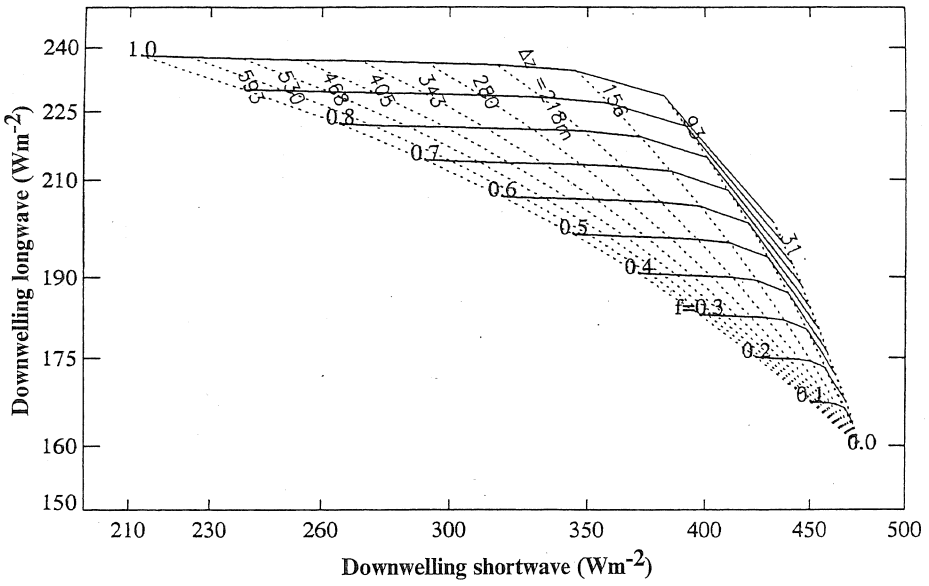

Figure 3. Downwelling broadband short- and longwave fluxes computed as a function of cloud fraction and physical thickness. Radiative transfer calculations were conducted using a subarctic winter atmospheric profile at a solar zenith angle of 58°. The following values are assumed constant: Cloud top height (725 mb), effective cloud droplet size (10 μm), liquid water concentration (0·2 gm^{-3}), and surface albedo (0·75).

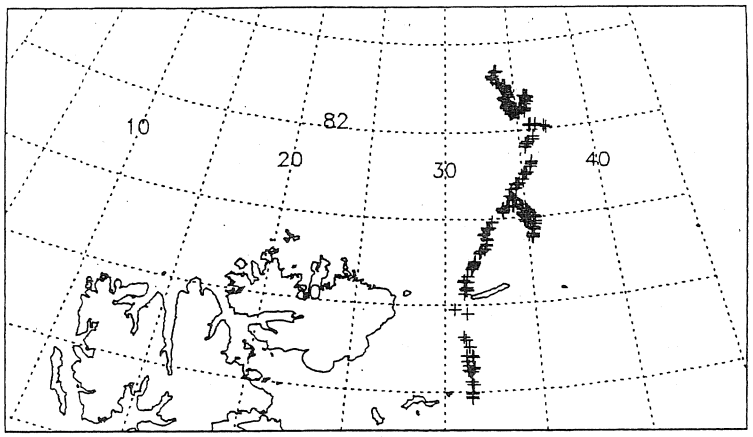

Figure 4. Locations of CEAREX camp.

radiation flux retrievals for conditions typical of a coastal station (hereafter referred to as CST). TOVS MSU and HIRS data for these periods were acquired from the National Center of Atmospheric Research (NCAR) and NOAA NESDIS and collocated with the ground measurements. HIRS and MSU brightness temperatures are preprocessed and interpolated to 'retrieval boxes' using the corresponding steps of the 3I algorithm. Preprocessing includes calibration for both channels and corrections for antenna pattern, limb effects and surface emissivity (except MSU1) for the MSU channels. (Chedin *et al.* 1985). Surface observations were matched with the closest

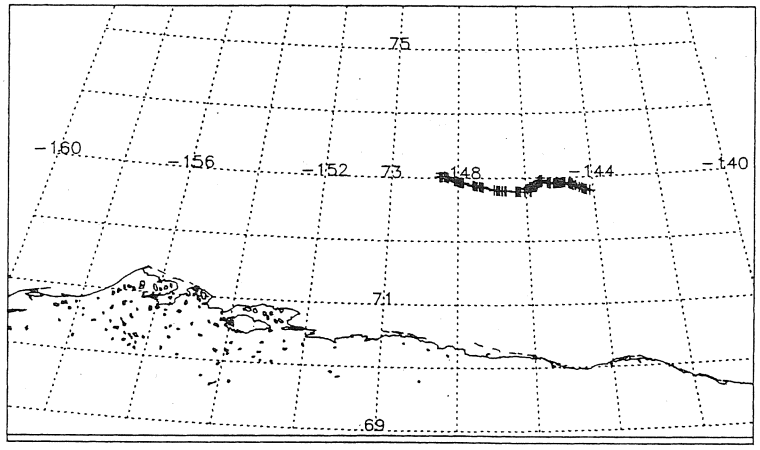

Figure 5. Locations of LeadEx camp.

retrieval box within a 200 km radius from the location of the surface station. Satellite and surface observations were allowed to be no more than 30 min apart (centre of the 1 h interval). The physically-based method for the computation of downwelling longwave fluxes (Francis 1995) was applied to a subset of the CEAREX data. This method combines the atmospheric temperature and humidity profiles computed using the 3I algorithm with cloud properties derived from HIRS channels to calculate downwelling longwave fluxes using a two-stream radiative transfer model. Physically-based results are used for comparison with the results of the neural network.

5. Results

5.1. *Results from ICE data set*

ICE data set training (315) and test (79) cases were randomly drawn without replacement from these observations. Results from all experiments are summarized in table 1, which gives the root-mean-square (r.m.s.) error, the mean error (ME), and the square of the correlation coefficient (R^2). Prior to training, data were scaled into the range 0·15 to 0·85. Using a learning rate (Rummelhart *et al.* 1986) of 0·1 and a momentum value of 0·05, the network was trained for 17 500 iterations before training was stopped because the error for the test data set began to rise and the network had reached its level of optimal generalization. Slowing the learning rate to 0.05 and

Table 1. Difference between observed and estimated surface radiative fluxes.

	Training cases	Test cases	Downwelling longwave			Downwelling shortwave		
			r.m.s.	ME	R^2	r.m.s.	ME	R^2
ICE	315	79	19·5	−2·36	0·72	25	0·05	0·97
LeadEx (trained on ICE)			14·9	0·07	0·82	34·8	1·3	0·96
CEAREX (trained on ICE)			22·51	−4·1	0·54	NA	NA	NA
Physical model (CEAREX)	NA	138	28·7	7·6	0·48	NA	NA	NA
ANN corresponding to above	NA	138	20·9	−0·8	0·62	NA	NA	NA
CST	716	180	20·15	−5·90	0·80	36·26	4·64	0·96

setting the momentum to 0 for the last 5000 cycles improved results slightly. After training, the network was applied to the test data set. Figures 6 and 7 show a comparison of observed and network-derived downwelling longwave (DWL) and shortwave fluxes (DWS) for the test cases. Error of r.m.s. for the DWL flux is 19·5 W m^{-2} with a mean error of −2·36 W m^{-2}. The variance in the surface observations explained by the ANN-based model is 72 per cent. The r.m.s. error for DWS fluxes for the combined ICE data set is 24·9 W m^{-2} with a mean error (ME) of 0·05 W m^{-2}. DWS results for the combined experiment are skewed because DWS for the majority of cases from the CEAREX data set are 0 during darkness. Results for the LeadEx cases were therefore computed separately using the network trained on the combined data. DWS r.m.s. errors for the LeadEx period alone are 34·8 W m^{-2} with a ME of 1·3 W m^{-2}. DWL errors for the LeadEx period are 14·9 W m^{-2} (r.m.s.) and 0·07 W m^{-2} (ME). DWL errors for the CEAREX period are 22·57 W m^{-2} (r.m.s.) and −4·1 W m^{-2} (ME). It is interesting to see that the errors in DWL fluxes for the LeadEx period are substantially smaller than for the CEAREX period. There are

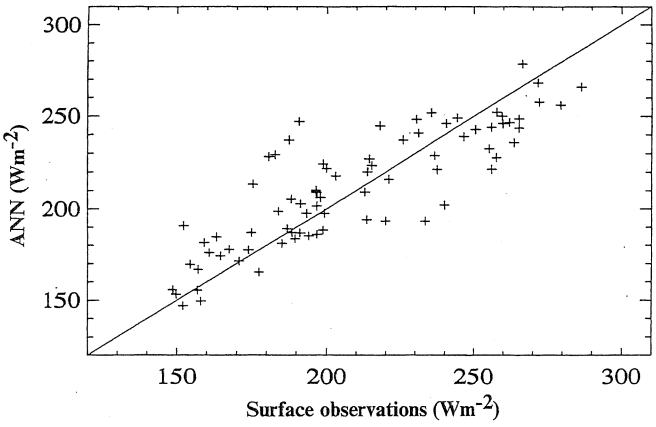

Figure 6. Comparison of downwelling longwave flux computed by the neural network vs. surface observations for the ICE data set.

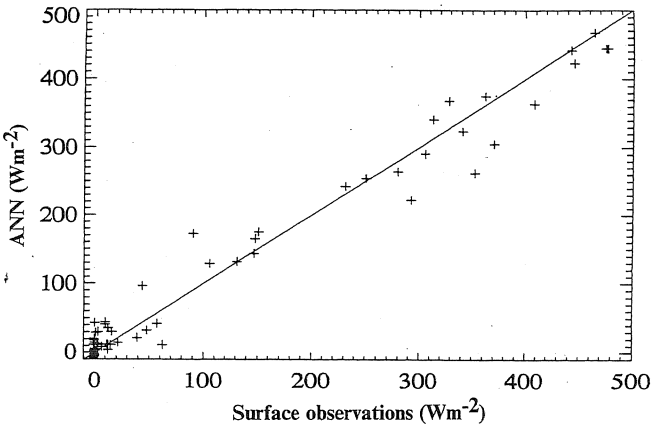

Figure 7. Comparison of downwelling shortwave flux computed by the neural network vs. surface observations for the ICE data set.

several possible explanations for this. Since the CEAREX period covers a longer time period, the range of possible conditions over which the network has to find a retrieval function is greater. Although the range in downwelling longwave fluxes is similar, temperature structure, cloud conditions and ice types are likely to vary over a greater range. Additionally, the larger proportion of downwelling shortwave fluxes in the LeadEx data may have provided constrains during training (see section 3.2) that resulted in a network that performs better when reflected solar radiation in visible and near-infrared channels is present.

Since the cosine of the solar zenith angle is one of the input variables, and the network clearly must exploit this strong relationship, it is interesting to ask what additional skill the network has acquired in retrieving DWS. Figure 8 shows the results of a simple regression model, where $\mathrm{DWS} = a + b\cos(\theta)$, where θ is the solar zenith angle. For the LeadEx data set, the r.m.s. error is $50\,\mathrm{W\,m^{-2}}$ with explained variance of 86 per cent. Comparing these results with the test data for the LeadEx period shows that the network reduces the error by $15\,\mathrm{W\,m^{-2}}$ (r.m.s.) and increases the explained variance by 10 per cent. Errors in DWS using the linear model naturally increase with greater values of DWS. Interestingly, the ANN retrieved DWS value do not show this trend. This is clear evidence that the ANN has indeed been able to interpret the TOVS brightness temperatures to make corrections for non-linear radiative processes.

Figure 9 shows a comparison of the ANN results with those of the physical model (Francis 1995). Since physical model retrieval is limited to cases where the 3I algorithm performs a retrieval, the case comparison is not identical to the test data set. However, none of the cases in this comparison had been used in the training of the ANN. Errors of DWL for the physically-based algorithm are $28\,\mathrm{W\,m^{-2}}$ (r.m.s.) and 7·6 (ME) vs. $21\,\mathrm{W\,m^{-2}}$ (r.m.s.) and -1 (ME). This demonstrates the superior

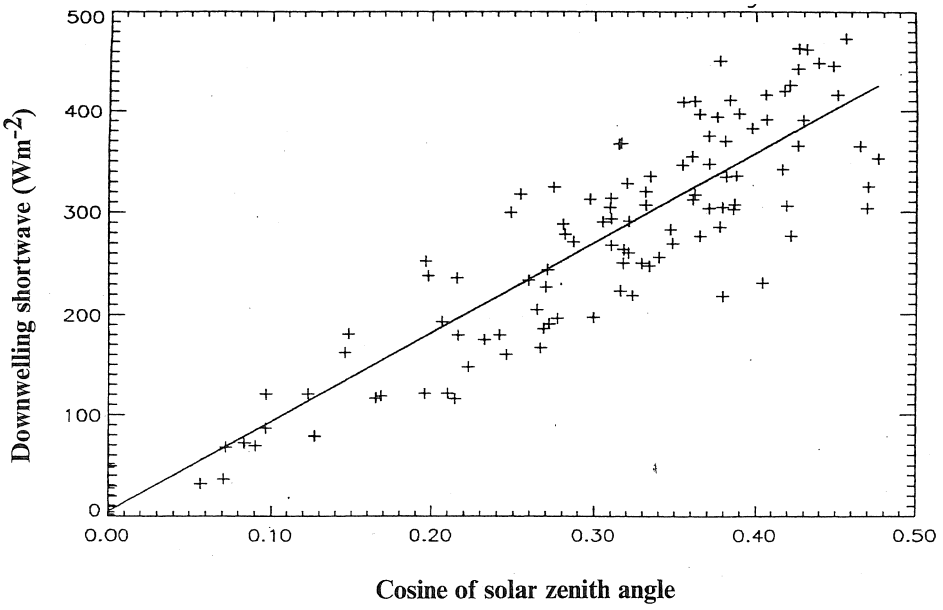

Figure 8. Comparison of downwelling shortwave flux computed by a linear model based on the cosine of the solar zenith angle and surface observations.

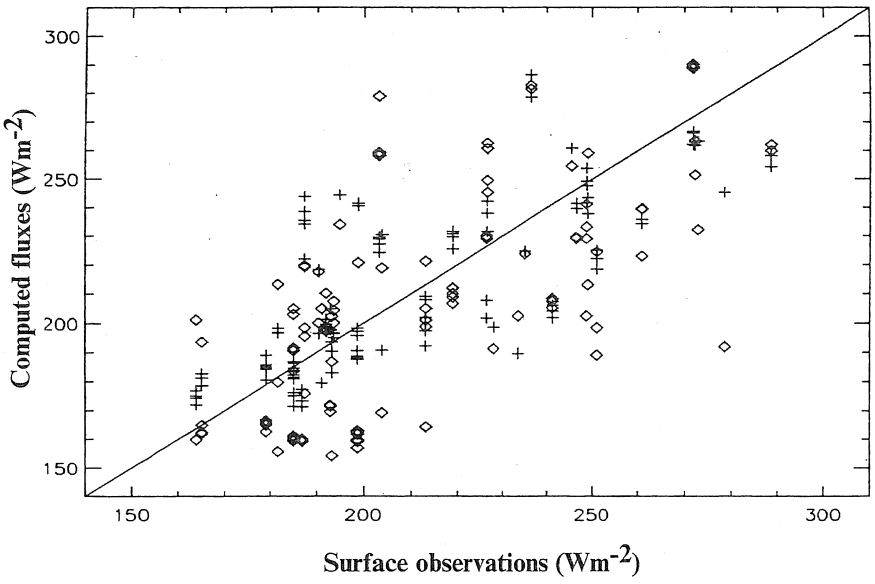

Figure 9. Comparison of downwelling longwave flux computed by the neural network (crosses) vs. the physical model of Francis (diamonds).

performance of the ANN over the physical method for the data and methods examined here.

5.2. *Results from the CST data set*

Barrow, the source of the CST data set, is located on a peninsula off the Alaska coast on the Beaufort Sea. Climatological conditions for the winter months at this location are similar to those found at the camps used for the ICE data set. However, from the perspective of the TOVS HIRS and MSU sensors with footprint sizes of 18 and 100 km, respectively, this location presents a problem. Within a single footprint one may find bare or snow-covered land, lakes, open ocean in a flaw-lead located near the coast and sea ice. Pairs of TOVS brightness temperatures and surface observations of DWL and DWS were separated into 716 training and 180 test cases. The network shown described in section 3.2, although with an increased number of hidden units (8), was trained using the CST data set. Results of the test data set are shown in figures 10 and 11.

Errors for DWS are 36·26 $W m^{-2}$ (r.m.s.) and 4·64 $W m^{-2}$ (ME) and for DWL 20·15 $W m^{-2}$ (r.m.s.) and $-5·90$ $W m^{-2}$ (ME). Using only four hidden units produced similar errors for DWL but increased the DWS r.m.s. to 45·03 $W m^{-2}$.

6. Discussion and conclusions

The results presented above are very encouraging and demonstrate the viability of the presented method. Mean retrieval errors (ME) are clearly within the desirable range for climate process studies. The point versus areal average nature of this comparison and the intrinsic error in the surface observations of radiation in the Arctic (e.g., frost covering of measurement dome) both contribute to the estimation error. Additionally, the coarse vertical resolution of the HIRS weighting functions makes this sensor 'blind' to certain atmospheric characteristics that affect the surface

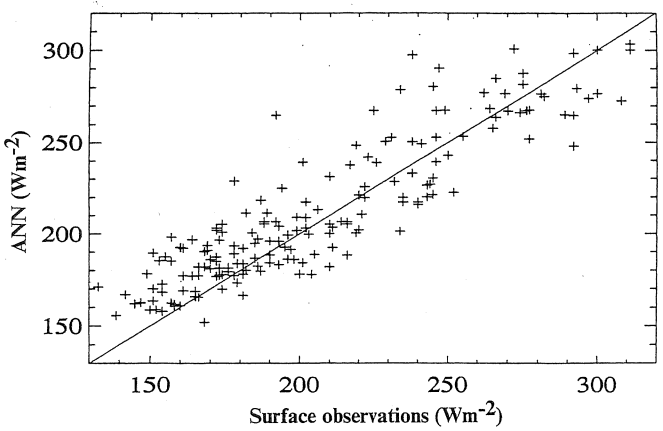

Figure 10. Comparison of downwelling longwave flux computed by the neural network vs. surface observations for the CST data set.

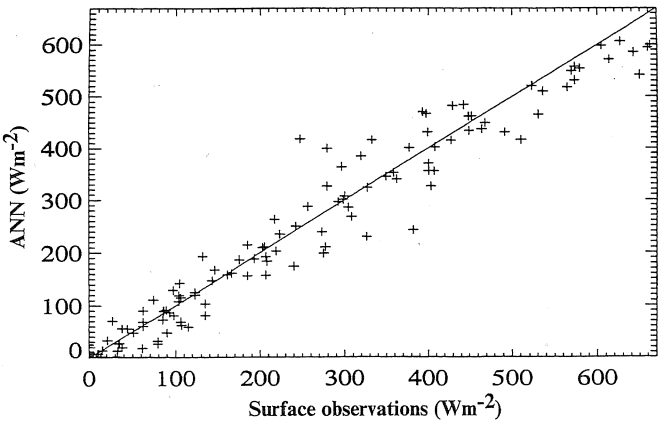

Figure 11. Comparison of downwelling shortwave flux computed by the neural network vs. surface observations for the CST data set.

radiative fluxes, e.g., low-level temperature inversions cannot be completely resolved. Of course, these error sources are not unique to the ANN method presented here, but are factors in physical retrievals as well.

The difficulty in comparing point measurements with 100 km satellite retrieval footprints is illustrated by the time auto-correlation function for DWL at the CEAREX camp (figure 12). Making the admittedly crude assumption that the variables affecting downwelling longwave radiation travel at the same speed as the wind (typical value for the Arctic 10 m/s), a 100 km distance corresponds to a time difference of approximately 3 h. Thus the temporal auto-correlation at a 3 h lag can be used as a rough estimate of the spatial auto-correlation at 100 km. At this time lag the auto-correlation of DWL drops to 0·7. For DWS (not shown), also affected by more variable surface conditions, the spatial variability is even greater.

Having demonstrated the method's performance for the four months of the ICE data set and the five months of the CST data set, we are now faced with the challenge to construct a network that performs the retrievals over the range of surface and

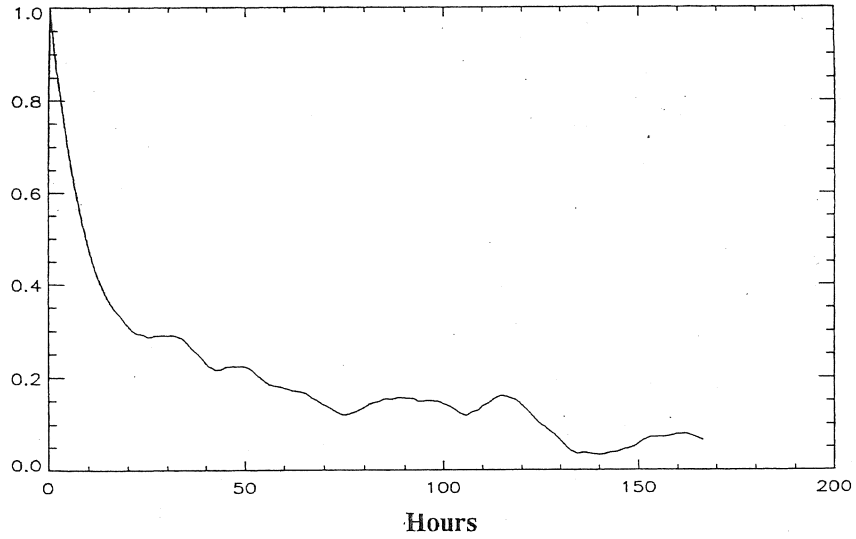

Figure 12. Temporal auto-correlation of downwelling longwave fluxes at the CEAREX camp.

atmospheric conditions that will be encountered within the domain of its intended application. As with any empirical method this is very important. Figure 13 illustrates one aspect of this problem. DWL calculated by the network that was trained on the CEAREX data exclusively and then applied to LeadEx data set. Errors of r.m.s. ($25\,W\,m^{-2}$) are similar to the results achieved for the CEAREX data but the mean error indicates a bias of $-12\,W\,m^{-2}$. This does not come as a great surprise. In addition to different environmental conditions (see section 5.1), we need to consider the fact that the TOVS instruments for NOAA-10 (CEAREX period) and NOAA-11 (LeadEx period) have different channel combinations. For example, channel 10 on NOAA-10 has a central wavelength of 8·3 μm, while on NOAA-11 it is 12·56 μm. Clearly such changes, as well as more subtle changes in the spectral response functions

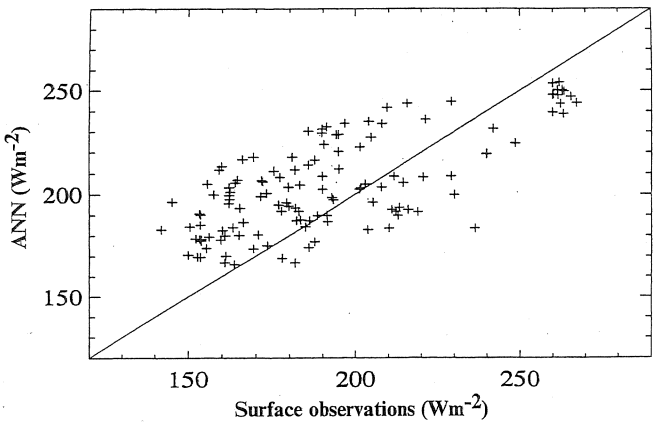

Figure 13. Comparison of downwelling longwave fluxes computed by a neural network which was trained on the CEAREX data set and applied to the LeadEx data set. Note that for the CEAREX period NOAA-10 data were used; for the LeadEx period NOAA-11 data were used.

and inaccuracies in the calibrations, need to be accounted for. We are currently approaching this problem from several angles. First, we are assembling a much larger data set from multidecadal measurements of surface radiation fluxes made on Russian drifting stations which will provide additional training data for central Arctic conditions. Second, we are also working on the generation of an artificial data set based on modelled TOVS brightness temperatures and DWL and DWS fluxes over a wide range of cloud conditions. Differences in sensor systems can be addressed through corrections in preprocessing steps. In addition, the upcoming year-long Arctic field experiment SHEBA (Moritz *et al.* 1993) will provide an excellent opportunity to obtain a training and validation data. Since radiatively relevant cloud properties will be measured, it will provide an opportunity to analyse how the neural network responds to changes in specific variables.

Acknowledgements

This work was supported by National Aeronautics and Space Administration (NASA) grants NAGW-4169 (RADNET), NAGW-3437, and NAGW-2407 (EOS-POLES). We would also like to acknowledge the National Center for Atmospheric Research (NCAR) for providing TOVS MSU and HIRS data for the CEAREX period and Peter Topoly (NOAA-SAA) for the access to TOVS data for the LeadEx period. K. Davidson and P. Guest are acknowledged for providing CEAREX surface radiation measurements. Jennifer Francis provided results of the DWL retrievals runs of her model for the CEAREX time period. Bob Stone is acknowledged for providing radiation data from Barrow. We thank the anonymous reviewers for valuable comments.

References

BUTLER, C. T. and MEREDITH, R. v. Z., 1992, Retrieving atmospheric temperature profiles from simulated DMSP sounder data with a neural network. Applications of artificial neural networks III, SPIE Transactions, **1709,** 780–788.

CEAREX DRIFT GROUP, 1990, CEAREX drift experiment. *American Geophysical Union Earth Observation System Transactions*, **71,** 1115–1118.

CHEDIN, A., SCOTT, N. A., WAHICHE, C. and MOULINIER, P., 1985, The improved initialization inversion method: a high resolution physical method for temperature retrievals from satellites of the TIROS-N series. *Journal of Climatology & Applied Meterology*, **24,** 128–143.

CLAUD, C., CHEDIN, A., SCOTT, N. A. and GASCARD, J. C., 1989, Retrieval of mesoscale meteorological parameters for polar latitudes (MIZEX and ARCTEMIZ campaigns). *Annals of Geophysics*, **7,** 205–212.

ESCOBAR, M. J., CHEDIN, A., CHERUY, F. and SCOTT, N., 1993, Multi-layer neural networks for the retrieval of atmospheric variables from satellite-borne vertical sounding. *Comptes Rendus de l'Academie des Sciences, Serie II (Mecanique, Physique, Chimie Sciences de la Terre et de l'Univers)*, **317,** 911–918.

FINNOFF, W., HERGERT, F. and ZIMMERMAN, H. G., 1993, Improving model selection by nonconvergent methods. *Neural Networks*, **6,** 771–783.

FRANCIS, J. A., 1994, Improvements to TOVS retrievals over sea ice and applications to estimating arctic energy fluxes. *Journal of Geophysical Research*, **99,** 10 395–10 408.

FRANCIS, J. A., 1995, TOVS-derived estimates of downwelling longwave radiation fluxes over the Arctic Basin. *Proceedings of the Fourth Conference on Polar Meteorology and Oceanography, Dallas, Texas, 15–20 January 1995* (Dallas: American Meteorological Society), pp. 43–46.

KERGOMARD, C., BONNELA, B. and FOUQUART, Y., 1993, Retrieval of surface radiative fluxes on the marginal zone of sea ice from operational satellite data. *Annals of Glaciology*, **17,** 201–206.

KEY, J. and BARRY, R. G., 1989, Cloud cover analysis with Arctic AVHRR data, 1. Cloud detection. *Journal of Geophysical Research*, **94,** 18 521–18 535.

KEY, J., MASLANIK, J. A. and SCHWEIGER, A. J., 1989, Classification of merged AVHRR and SMMR arctic data with neural networks. *Photogrammetric Engineering and Remote Sensing*, **55,** 1331–1338.

KEY, J., 1996, *Streamer User's Guide.* Technical Report 96-01, Department of Geography, Boston University, 85 pp.

KEY, J. and STONE, R. S., 1995, Accuracies of satellite-derived cloud and surface parameters in the polar regions and their effect on radiative flux estimates. *Proceedings of the Fourth Conference on Polar Meteorology and Oceanography, January 1995*, American Meteorological Society, Dallas, pp. 32–37.

KIDWELL, K. B., 1995. Polar Orbiter Data Users Guide. National Oceanic and Atmospheric Administration, National Environmental Satellite, Data, and Information Service.

LEADEX GROUP, 1993, The Lead Experiment, *American Geophysical Union Earth Observation System Transactions*, **74,** 393–397.

LEE, J. R., WEGER, C., SENGUPTA, S. K. and WELCH, R. M., 1990, A neural network approach to cloud classification. *I.E.E.E. Transactions on Geoscience & Remote Sensing*, **28,** 846–855.

MORITZ, R. E., CURRY, J. A., THORNDIKE, A. S. and UNTERSTEINER, N., (eds). 1993, Surface heat budget of the Arctic Ocean. Arctic System Science, Ocean Atmosphere Interactions Report No. 3. University of Washington, Applied Physics Laboratory.

MORCRETTE, J. J. and DESCHAMPS, P. Y., 1986, Downward longwave radiation at the surface in clear-sky atmospheres: comparison of measured, satellite-derived and calculated fluxes. *Proc. ISLSCP Conf., Rome, Italy, 2–6 December 1985*, ESA SP-248 (Noordwijk: European Space Agency), pp. 257–261.

NAKAJIMA, T. and KING, M. S., 1990, Determination of the optical thickness and effective particle radius of clouds from reflected solar radiation measurements. Part I: theory. *Journal of Atmospheric Science*, **47,** 1878–1893.

OVERLAND, J. E. and GUEST, P. S., 1991, The arctic snow and air temperature budget over sea ice during winter. *Journal of Geophysical Research*, **96,** 4651–4662.

RODGERS, C. D., 1976, Retrieval of atmospheric temperature and composition from remote measurements of thermal radiation. *Review of Geophysics & Space Physics*, **14,** 609–624.

ROSSOW, W. B. and ZHANG, Y. C., 1995, Calculation of surface and top of atmosphere radiative fluxes from physical quantities based on ISCCP data sets. 2. Validation and first results. *Journal of Geophysics Research*, **100,** 1167–1197.

RUFFIEUX, D., OLA, P. and PERSSON, G., 1995, Ice pack and lead surface energy budgets during LeadEx 1992. *Journal of Geophysical Research*, **100,** 4593–4612.

RUMMELHART, D. E., HINTON, G. E. and WILLIAMS, R. J., 1986, Learning internal representation by error propagation. In *Parallel Distributed Processing: Explorations in the Microstructure of Cognition*, edited by D.E. Rummelhart and J.L. McCleland (Cambridge, MA: MIT Press), pp 318–362.

SCHMETZ, J., 1989, Towards a surface radiation climatology: retrieval of downward irradiances from satellites. *Atmospheric Research*, **23,** 287–321.

SCHWEIGER, A. J. and KEY, J. R., 1994, Arctic Ocean radiative fluxes and cloud forcing estimated from the ISCCP cloud data set, 1983–1990. *Journal of Applied Meteorology*, **33,** 948–963.

TOVINKERE, V. R., PENALOZA, M., LOGAR, A., LEE, J., WEGER, R. C., BERENDES, T A. and WELCH, R. M., 1993, An intercomparison of artificial intelligence approaches for polar scene identification. *Journal of Geophysical Research*, **98,** 5001–5016.

WORLD MARITIME ORGANIZATION/WORLD CLIMATE RESEARCH PROGRAMME, 1992, Arctic Climate System Study (ACSYS). Report of the JSC Study Group, JSC XIII/Doc 5. Annex.